Journal of Catalysis **188,** 48–57 (1999)
Article ID jcat.1999.2596, available online at http://www.idealibrary.com on IDEAL®

Gas-Phase Oxidation of 1-Butene Using Nanoscale TiO_2 Photocatalysts

Lixin Cao, Aimin Huang, Franz-Josef Spiess, and Steven L. Suib[1]

U-60, Department of Chemistry, University of Connecticut, Storrs, Connecticut 06269-4060

Received January 13, 1999; revised May 17, 1999; accepted June 10, 1999

The effects of preparation methods, humidity, and calcination temperatures on the behavior of nanoscale TiO_2 photocatalysts were investigated in this study. Application of these photocatalysts in the gas-phase decomposition of 1-butene demonstrated that the nanoscale catalysts, prepared by the acid-assisted sol–gel technique, showed higher photocatalytic reactivity than commercially available Degussa P-25 TiO_2, while lower photoactivity was obtained on TiO_2 catalysts prepared without adding acid to titanium isopropoxide. Our experimental results revealed that the oxidation rates of 1-butene decreased exponentially with increasing water concentrations in the flowing stream. However, a trace amount of water vapor was indispensable in maintaining the stability of the catalysts. Proper calcination temperature (300°C) could promote the resistance of catalysts against the poisoning effects of humidity. Higher calcination temperature (400°C) unfavorably lowered the photoactivity due to phase transformations occurring at such a temperature. Amorphous and rutile-typed TiO_2 showed less photocatalytic reactivity. XRD patterns and BET measurements indicated that moderate surface areas (from 100 to 160 m^2/g), appropriate crystallite sizes (5 ~ 6 nm), and crystallinity of anatase were beneficial to the photoactivity of TiO_2 catalysts. *In situ* FTIR studies indicated that catalyst surfaces contained large amounts of chemisorbed water and hydroxyl groups, which are considered to be active sites in photocatalytic reactions. The accumulation of carbonate species on active sites resulted in the deactivation of TiO_2 catalysts under dry conditions. Quantum size effects were thought to be responsible for the high photoactivity achieved on the nanoscale TiO_2 catalysts prepared by sol–gel methods.

INTRODUCTION

Photocatalytic degradation of toxic organic chemicals has been widely studied in the past two decades since people have gradually realized the severity of environmental pollution. A great deal of work has been devoted to decontamination of air and water (1–3). Earlier publications mainly deal with the treatment of waste water. In recent years, air purification has attracted many researchers' interests (4, 5). An effective technique for this practice is to apply semiconductors as catalysts for decomposition of air contaminants with the assistance of UV or visible light. Commercially available Degussa P-25 TiO_2 has been extensively investigated because of its high photoactivity, stability, and low cost. Very few catalysts have been discovered that show higher photoactivity than P-25 TiO_2. Consequently, a significant improvement in the photoactivity of these semiconductors is still in need for the use of this technology in industry. However, three crucial factors tremendously inhibit the photoactivity:

(1) Recombination of electrons and holes. In general, semiconductors can absorb photons to generate electrons in the conduction band and holes in the valence band. Oxygen and organic compounds then capture electrons and holes, respectively, to form two types of radicals, which subsequently lead to destruction of the pollutants. A competitive process involves recombination of electrons with holes to give off heat or luminescence. The recombination process proceeding in the same time scale as redox processes significantly reduces the photoactivity of semiconductors (6, 7).

(2) Negative effects of gaseous water on photoactivity of catalysts. Various photocatalytic reactions proceed efficiently using TiO_2 photocatalysts in aqueous systems (1). The water concentration in the gas phase significantly influences the photocatalytic reactivity in gas–solid reactions. Anpo *et al.* (8) have claimed that the addition of water onto oxides (TiO_2 and ZnO) causes structural changes in surface band bending, which enhances the efficiency of electron–hole recombination, and thus reduces photoefficiency. Phillips and Raupp (9), Peral and Ollis (10), and Obee and Brown (11) have reported that competitive adsorption of water on TiO_2 surfaces may be associated with the low photoefficiency since hydroxyl groups are considered to be active sites (12). Anyhow, the high humidity of the atmosphere (varies with seasons and temperatures, generally about 10,000 ppm) is a big challenge for application of this technology.

(3) Deactivation. Although no deactivation was reported in aqueous reactions (a possible reason is that batch reactors have been used in such experiments), many authors (10, 13–15) observed deactivation of their catalysts in gas-phase reactions. Some side products, for instance, carboxylic acids formed in the incomplete oxidation of organic compounds, can be chemisorbed on active sites. The white

[1] To whom correspondence should be addressed.

0021-9517/99 $30.00

P-25 TiO_2 can turn yellow after reaction. Thus, the lifetime of the catalysts is still a serious problem.

Therefore, new types of photocatalysts should be developed to overcome the above weaknesses. Previously, we have synthesized nanocrystalline SnO_2 catalysts for the oxidation of 1-butene. The SnO_2 films show much higher photoactivity than P-25 TiO_2, but they can not tolerate high humidity (>3000 ppm). In this paper, using different methods, we prepared three types of TiO_2 catalysts for the oxidation of 1-butene. P-25 TiO_2 was chosen to be the reference catalyst for comparison with the prepared catalysts. The catalyst produced by adding hydrochloric acid to hydrolyze titanium isopropoxide and calcined at 300°C shows much higher photoactivity than P-25 TiO_2 in a wide range of water concentrations (2,250 to 12,000 ppm). Deactivation of these catalysts was observed only under conditions of low water concentration (<2000 ppm). In addition, XRD, BET, and FTIR techniques were employed to characterize the properties of these catalysts.

EXPERIMENTAL SECTION

Catalyst Preparation

For simplicity, we use four sets of codes to represent the four series of catalysts in this paper, as follows: TiA, commercially available Degussa P-25 TiO_2; surface area, ~50 m^2/g; primary particle size, 30 nm; band gap, 3.2 eV; anatase : rutile = 70 : 30 (1).

TiB. Deionized distilled water (DDW) was used to hydrolyze titanium isopropoxide. Forty milliliters anhydrous ethanol was used to dilute 8 g $Ti[OCH(CH_3)_2]_4$. The ethanol–water mixture (30 mL ethanol and 30 mL DDW) was then added to the titanium isopropoxide solution, dropwise and with vigorous stirring. A white TiO_2 precipitate was immediately produced. The solvent was then evacuated. The precipitant was calcined at 120 and 300°C for 12 h to obtain TiB1 and TiB2 catalysts, respectively.

TiC. DDW and nitric acid were used to hydrolyze titanium isopropoxide (sol–gel process). The procedures for preparing the TiC catalysts were similar to those for TiB catalysts. Instead, eight drops of concentrated nitric acid (~70 wt%) were added to a water–ethanol mixture. A sol–gel was formed after hydrolysis of titanium isopropoxide, and then the resultant solution was aged for 1 day at room temperature. After the solution was condensed, the solvent was evacuated. The gel was calcined at 120 and 300°C for 12 h to produce TiC1 and TiC2 catalysts, respectively.

TiD. DDW and hydrochloric acid were used to hydrolyze titanium isopropoxide. The sole difference between the preparation of TiC and TiD series catalysts was the replacement of HNO_3 with concentrated HCl (~37 wt%) in the formation of TiD. The gel was calcined at 120, 200, 300, and 400°C for 12 h to produce TiD1, TiD2, TiD3, and TiD4 catalysts. For comparison, the hydrolyzing regents and the calcination temperatures are listed in Table 1.

TABLE 1

Nomenclature and Preparation Methods of Different Catalysts

Catalyst code	Hydrolyzing regent	Calcination temperature (°C)
TiA (P-25 TiO_2)	—	—
TiB1	H_2O	120
TiB2	H_2O	300
TiC1	$H_2O + HNO_3$	120
TiC2	$H_2O + HNO_3$	300
TiD1	H_2O + HCl	120
TiD2	H_2O + HCl	200
TiD3	H_2O + HCl	300
TiD4	H_2O + HCl	400

Film Preparation

The materials obtained from the above procedures were ground to fine powders. The powdered samples were mixed with distilled water to make slurry-like suspensions, which subsequently were coated on microscope glass slides (7.5 cm × 1.8 cm). The loading of catalysts on glass slides was approximately 2.5 mg/cm^2. Films with such high loadings are thick enough to prevent UV light from penetrating the slides (16).

Apparatus

Oxidation rates of 1-butene presented in this paper were directly obtained in a glass-plate photocatalytic reactor since the reactor was operated as a differential reactor under conditions of high flow rates (3.6 L/min) and low conversions of 1-butene (<20%) (17). The inlet concentration of 1-butene was 2.75 ppm throughout this study. UV illumination was generated with a pair of black-light lamps ($\lambda > 300$ nm, 352-nm peak intensity, SpectroLine XX-15A). UV intensity at the catalyst surface was measured with a UVA power meter (Oriel UVA Goldilux) and was 0.70 mW/cm^2. Nitrogen passed through a water bubbler to obtain different water vapor levels in the feed stream. An oxygen gas flow mixed with nitrogen and 1-butene produced the desired carrier gas mixture. A GC (HP-5890 II) equipped with an FID detector and an RTX-1 column (RESTEK Corp.) were used to measure inlet and outlet concentrations of 1-butene. The concentrations of water were determined using a photoacoustic detector (Brüel & Kjær 1302). These experiments were done at room temperature and approximately atmospheric pressure.

Characterization Methods

X-ray powder diffraction (XRD) experiments were carried out on a Scintag Model PDS 2000 diffractometer.

Samples were loaded on glass slides, and Cu $K\alpha$ radiation was used at 45 kV and 40 mA. The sample scans were collected between 5° and 60° 2θ. X-ray line broadening analysis (LBA) is useful in estimating average particle sizes (18). Particles up to about 100 nm cause broadening of the diffraction lines. The extent of broadening is given by the Scherrer equation

$$t = 0.9\lambda/(B\cos\theta_B), \quad [1]$$

where λ is the wavelength of X-rays (1.54060 Å for Cu $K\alpha$ radiation), B is the broadening of diffraction lines measured at half of the maximum intensity (radians), θ_B is the angle of diffraction corresponding to the peak broadening, and t is the diameter of the particle. LBA is believed to be applicable in the range of about 1.5 to 100 nm (19).

Diffusion reflectance Fourier transform infrared (FTIR) spectroscopy experiments were performed on a Nicolet 750 spectrometer with a Mercury–Cadmium–Telluride (MCT) detector and KBr beam splitter. The *in situ* IR experiments were done with a heating attachment. The heating temperature was varied from 25 to 350°C. Spectra were collected with a resolution of 4 cm^{-1} by using 100 scans.

Surface area measurements were obtained with the BET method by using N_2 gas in a Quantachrome Nova-1000 apparatus. The samples were preheated for 1 h at 120°C before the measurement.

RESULTS

The volumetric flow rate in this study was kept at 3.60 L/min. Under such high flow rates, the effect of external mass transfer is negligible. The reaction rates thus represent the intrinsic chemical kinetics of surface reactions. The experiments were performed at room temperature and atmospheric pressure. Under these conditions, the reaction rate of 1-butene for each run can be expressed as

$$r = 0.654\chi C_{B0}/N, \quad [2]$$

where r (μmol/cm^2 h) is the oxidation rate, χ is the conversion of 1-butene, C_{B0} is the inlet concentration of 1-butene, and N is the number of slides used for the reaction. In the present study, the area of each slide is 13.5 cm^2, and C_B is 2.75 ppm.

Photoactivity of Catalysts

Figure 1 gives the oxidation rates of 1-butene in the absence of water in the feed stream. In this case, the carrier gas bypassed the water bubbler, which was used to vary water levels. The gas flows thus were free of water vapor. The photoactivity, measured by the oxidation rate of 1-butene on different catalysts, is in the order TiD1 > TiC1 > TiA > TiB1. TiD1 and TiC1 (both were prepared by hydrolyzing titanium isopropoxide with HCl and HNO_3)

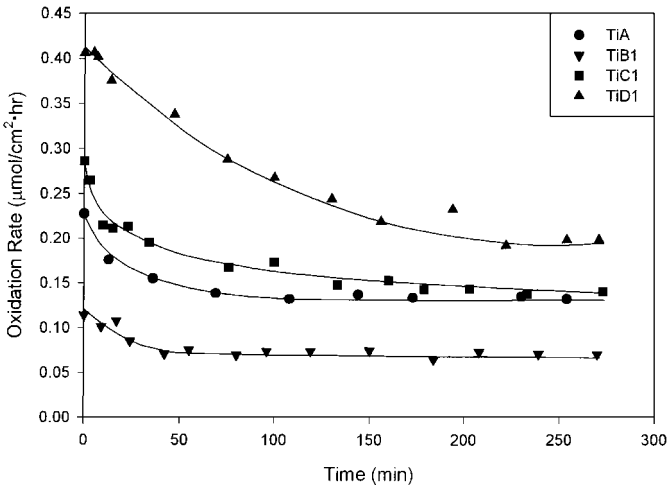

FIG. 1. Dependence of the oxidation rate of 1-butene versus time in the absence of water vapor, $I_0 = 0.70$ mW/cm^2, flow rate = 3.6 L/min, $C_{B0} = 2.75$ ppm.

show higher activity than P-25 TiO_2, which has been accepted to be a standard for most photocatalytic reactions (20). However, TiB1 (without using acid in the hydrolysis process) has poor activity. In comparison with the four catalysts, the sol–gel technique can be utilized to improve TiO_2 activity.

Figure 1 also shows that these catalysts lost their activity in the beginning of the reaction. After a certain period, each catalyst achieved a steady state in which no obvious deactivation took place. However, we observed that catalysts turned pale yellow after runs of 4.5 h. The vent gases were cooled to −78°C in order to trap side products, for instance, aldehydes, carboxylic acids, or ketones. However, no such partially oxidized products were detected by using GC-MS. We also attempted to extract adsorbed compounds from the used catalysts by using methanol as solvent. Nothing was found although FTIR results confirmed the presence of adsorbed species as shown in the spectra of Fig. 10. The reactant, 1-butene, had a very low concentration (~2.75 ppm) in the flowing stream. At such low levels, CO_2 cannot be determined quantitatively using a GC equipped with a TCD. For the photooxidation of ethylene and propylene (21), CO_2 has been reported to be the main product despite the observation of formaldehyde. Anpo *et al.* (8, 22) report that CO and CO_2 are major products in the oxidation reaction of alkynes and alkenes. On the basis of these reports, CO_2 is thought to be the major product in this study.

Realizing that the deactivation could be mainly due to the absence of water in the flowing stream, small amounts of water were added to the gas flow. The data obtained under such a condition are shown in Fig. 2; the water concentration was controlled at 2,250 ppm. The oxidation rates on different catalysts were stable after low water levels were introduced to the flowing stream. The sequence of photoactivity

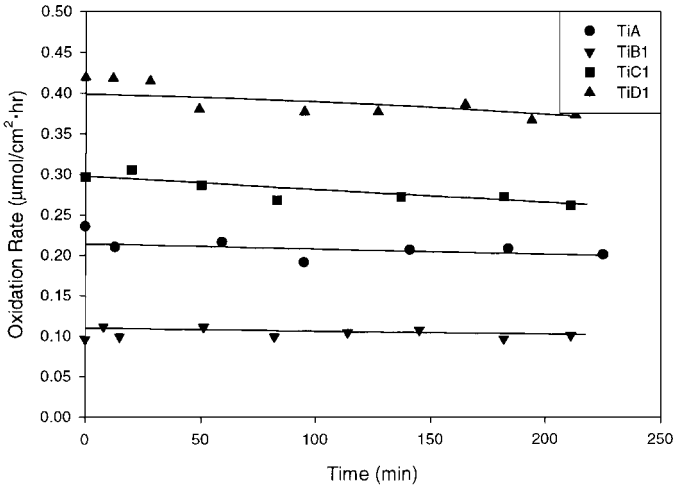

FIG. 2. Dependence of the oxidation rate of 1-butene versus time at a water concentration of 2250 ppm, $I_0 = 0.70$ mW/cm^2, flow rate = 3.6 L/min, $C_{B0} = 2.75$ ppm.

is still in the order TiD1 > TiC1 > TiA > TiB1. The oxidation rates on each catalyst are in accord with the initial oxidation rates of Fig. 1. The observation that small amounts of water vapor can promote and stabilize photoactivity is in agreement with the report of Phillips *et al.* (9). Thus, trace amounts of water can stabilize the photoactivity of TiO_2 catalysts.

Effects of Humidity

In order to further investigate the effects of humidity on photoactivity, the water concentration was varied over a large scale from 2,250 to 11,000 ppm (Fig. 3). No loss of activity was observed if the water concentration was higher than 2,250 ppm even though the white TiO_2 turned pale yellow after each use. Thus the data points in Fig. 3 represent steady state conversions. Figure 3 illustrates that photocatalytic activity of each catalyst plummets with increasing water concentration. Humidity tremendously influences the activity of TiC1 and TiD1 catalysts. P-25 TiO_2 (TiA) is not as susceptible to humidity as TiC1 and TiD1. At a water concentration of 11,000 ppm, TiA has the highest photoactivity although its oxidation rate is only half that of TiD1 at a water concentration of 2,250 ppm. TiB1 almost completely loses its activity at high water levels. The poisoning effects of gaseous water on photoefficiency for gas–solid reactions have been reported previously (8–11). For decomposition of 1-butene at high humidity levels, water is therefore a strong inhibitor.

Effects of Calcination Temperatures

As indicated in Fig. 3, humidity strongly affects the behavior of catalysts in this reaction. Considerable loss of photoactivity at high water levels is probably due to the affinity of catalyst surfaces to water since water is more polar than 1-butene. A possible improvement of resistance against humidity for the TiO_2 catalysts depends on pretreatment of catalyst surfaces (23). This is because the calcination temperature can alter surface properties, as well as catalyst structures. On the basis of this speculation, the TiB, TiC, and TiD series catalysts were calcined at different temperatures (Table 1). Since P-25 TiO_2 has been treated at high temperature (>1200°C) during the course of its preparation (3), no more calcination is needed for its study.

The behavior of the pretreated catalysts in the oxidation of 1-butene is shown in Figs. 4–6. Figure 4 shows enhancement of photoactivity with calcination temperatures (from 120 to 300°C). However, continuously increasing calcination temperature (400°C) gives rise to lower photoactivity

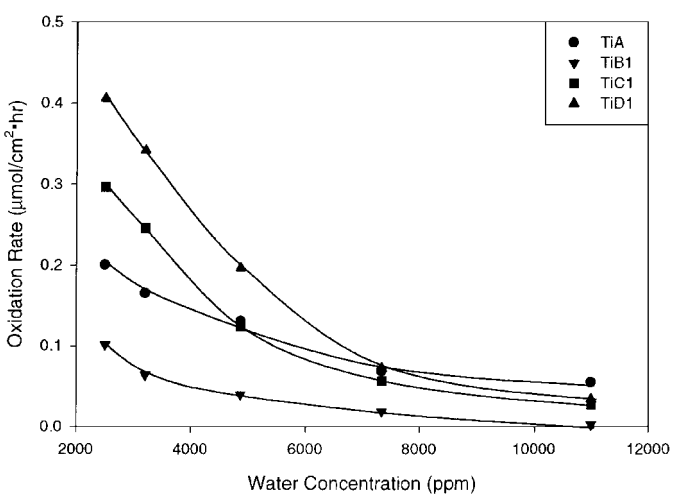

FIG. 3. Dependence of the oxidation rate of 1-butene on water concentration, $I_0 = 0.70$ mW/cm^2, flow rate = 3.6 L/min, $C_{B0} = 2.75$ ppm.

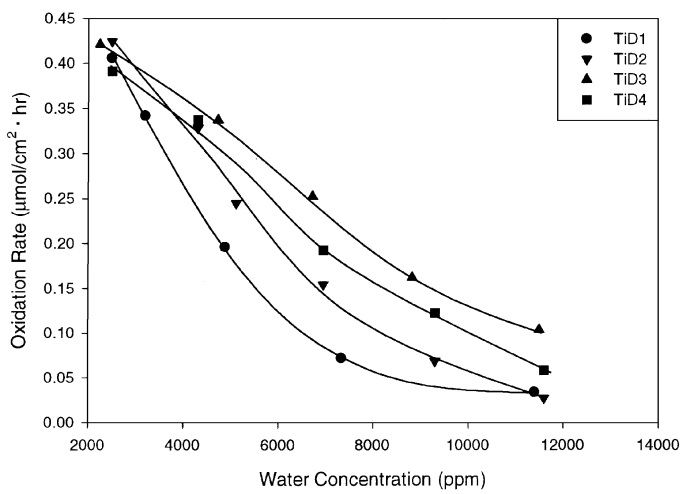

FIG. 4. Effect of water concentration on the oxidation rate of 1-butene for TiD series catalysts, $I_0 = 0.70$ mW/cm^2, flow rate = 3.6 L/min, $C_{B0} = 2.75$ ppm.

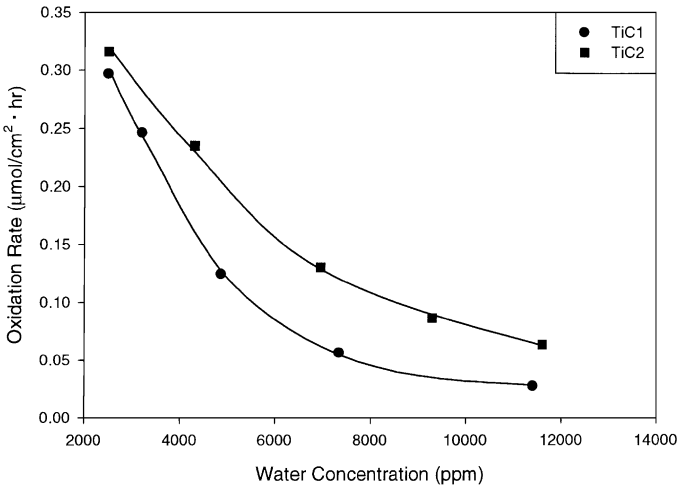

FIG. 5. Effect of water concentration on the oxidation rate of 1-butene for TiC series catalysts, $I_0 = 0.70$ mW/cm^2, flow rate = 3.6 L/min, $C_{B0} = 2.75$ ppm.

(TiD4). It turns out that a calcination temperature of 300°C enhances photoactivity. Compared with P-25 TiO_2 (TiA in Fig. 3), TiD3 has extraordinary activity even though humidity is still significantly detrimental to photoactivity. At a water concentration of 11,000 ppm, TiD3 gives an oxidation rate of 0.104 μmol/cm^2 h, while TiA gives 0.055 μmol/cm^2 h. Similarly, the calcination temperature is beneficial to TiB2 and TiC2 catalysts (Figs. 5 and 6). Therefore, appropriate calcination temperature is needed to maintain photoactivity in the presence of high water concentration.

XRD Patterns

XRD patterns for the catalysts are shown in Fig. 7. The structures and computed particle sizes are given in Table 2.

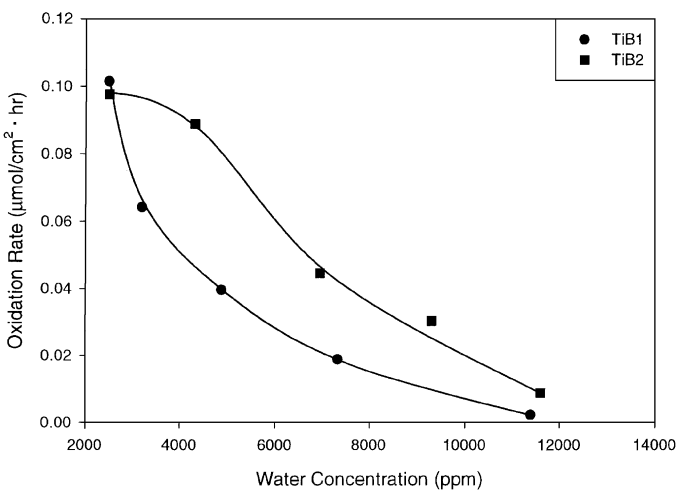

FIG. 6. Effect of water concentration on the oxidation rate of 1-butene for TiB series catalysts, $I_0 = 0.70$ mW/cm^2, flow rate = 3.6 L/min, $C_{B0} = 2.75$ ppm.

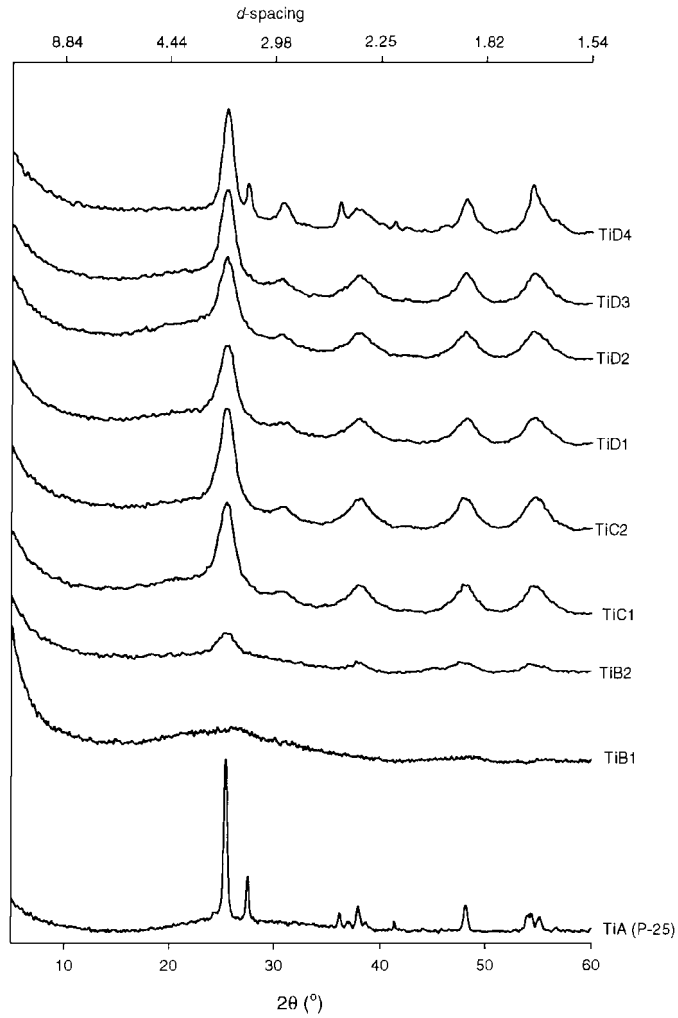

FIG. 7. X-ray diffraction patterns for TiA, TiB, TiC, and TiD series catalysts. The *d*-spacings of 3.52 and 3.25 are typical peaks for anatase and rutile, respectively.

TABLE 2

The XRD and BET Measurements for Different Catalysts

Catalyst	XRD results	Average particle size (nm)	Surface area (m^2/g)
TiA (P-25 TiO_2)	A : R (3 : 1)[a]	28.0	49
TiB1	AM	—	334
TiB2	AM + A	3.2	247
TiC1	A	4.8	157
TiC2	A	5.5	142
TiD1	A	4.9	155
TiD2	A	5.1	151
TiD3	A	5.9	134
TiD4	A + R	7.9	96

Note. A stands for anatase, R for rutile, and AM for amorphous TiO_2.
[a] The value is given in the literature (3).

The reference compound, P-25 TiO_2 (TiA), has two types of crystallinity, anatase (*d*-spacing of 3.52) and rutile (*d*-spacing of 3.25). TiB1 does not reveal regular crystallinity. TiB1 may be amorphous TiO_2. However, after TiB1 was calcined at 300°C, some of the amorphous TiO_2 was converted to anatase.

Both TiC1 and TiC2 catalysts mainly contain anatase. The calcination temperature only slightly increases the intensity of the peaks and narrows the broadness of the peaks. TiD series catalysts have the same structure as TiC catalysts. By comparison of TiD4 with TiA, the difference is that the TiD4 sample, calcined at 400°C, contains small amounts of rutile, which has a typical reflection with a *d*-spacing of 3.25. Fu *et al.* (24) have shown that TiO_2 samples prepared with sol–gel methods undergo a phase transformation from anatase to rutile beginning at 200°C. In this study, the phase transformation only happened to the sample calcined at 400°C. Using the Scherrer equation for X-ray line broadening and a computer program to determine *B* in Eq. [1], average particle sizes were determined, 28.0 nm for TiA and 4.8 ~ 8 nm for TiC and TiD series samples. The particle size value for TiB1 is not available since the Scherrer equation can not be used for calculation of amorphous systems. Table 2 summarizes the enhancement in particle size with calcination temperature. Thus, calcination temperature slightly causes agglomeration of particles.

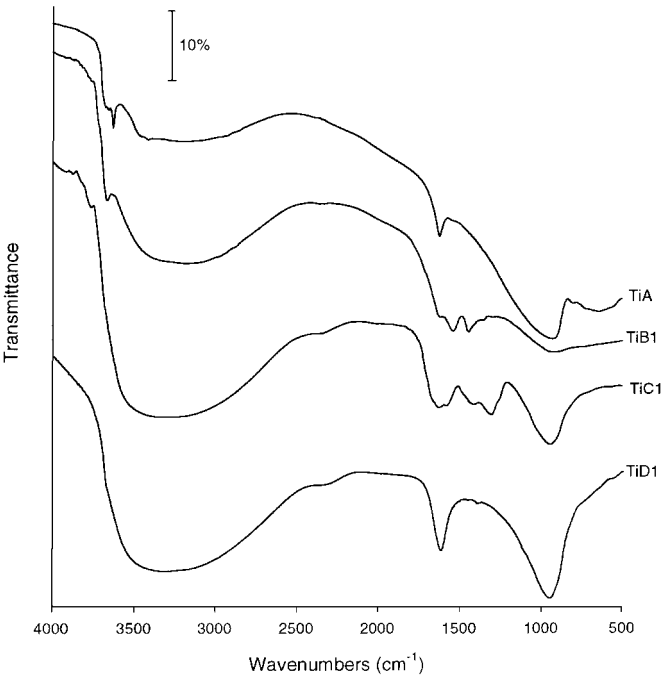

FIG. 8. Diffusion reflectance FTIR spectra of samples TiA, TiB1, and TiD1. Spectra were collected at room temperature.

Surface Area Analysis (BET)

Although the XRD patterns of TiB2, TiC, and TiD series catalysts are similar, their surface areas are different. Table 2 gives the results of BET measurements. The surface area of P-25 TiO_2 (49 m^2/g) is very close to the value given in the literature (25). TiB1 and TiB2 samples exhibit high surface areas. The surface areas of TiC and TiD series catalysts do not vary very much. The effect of the calcination temperature is obvious. The surface areas decrease with increasing calcination temperatures, in particular for TiB2 and TiD4 (400°C). The changing tendency of BET results is consistent with that of the XRD patterns. The particles of TiB1 are too tiny to exhibit crystallinity. Correspondingly, it has high surface area. Samples TiC1, TiC2, TiD1, TiD2, and TiD3, which have similar XRD patterns and particle sizes of 5 ~ 6 nm, have similar surface areas. For the TiD4 sample, in which anatase was partially converted to rutile during the annealing process, the surface area decreased significantly after it was calcined at relatively high temperature (400°C), and its particle size obviously increased. By relating surface areas to photocatalysis data, these data indicate that appropriate surface areas are critical for high photoactivity of TiO_2 catalysts. Too high or too low surface areas will result in poor photoactivity.

Anpo *et al.* (26) have reported that TiO_2 with a surface area as high as 1068 m^2/g was prepared by hydrolyzing $TiCl_4$. However, low surface areas (100–400 m^2/g) were obtained on TiO_2 synthesized with sol–gel methods (24, 27).

FTIR Data

Surface structure is important in these heterogeneous reactions since the interaction of reactants with surface active sites strongly influences the reaction rate. For the TiO_2 photocatalytic reactions, hydroxyl groups on the titania surface are active sites. The FTIR spectra of Fig. 8 show that sharp peaks appearing around 3650 cm^{-1} on TiA and TiB1 are assigned to "free" −OH stretching vibration (28). There are two types of −OH bands on TiA (3633 cm^{-1}, 3674 cm^{-1}), as some authors have observed (28). Hydroxyl stretching vibrations of molecularly adsorbed water are found around 3300 cm^{-1} and are represented by a very broad and intense peak. Correspondingly, the strong absorption band at 1627 cm^{-1} is the bending mode of molecular water. The weak frequency at 2305 cm^{-1}, which appears only on TiD1, is the combination band of 1627 and 678 cm^{-1} (very weak) (29, 30). The Ti–O vibration band is at 950 cm^{-1}. Two peaks in the region of 1400 to 1600 cm^{-1} on TiB1 probably arise from contaminants adsorbed on TiO_2 surfaces. The TiC1 spectra confirm the presence of NO_3^- on TiO_2 surfaces since this sample was prepared by adding HNO_3 to catalyze the sol–gel process. In comparing the relative intensities of molecular water bands, catalysts hydrolyzed by adding acids (TiC1 and TiD1) contain more water than TiA and TiB catalysts. If the typical hydroxyl groups are considered to be active sites, it is expected that the band of

free hydroxyl groups should be present on the TiD1 sample since TiD1 shows high photoactivity in Fig. 1. Yet, no apparent band of free hydroxyl groups is present on TiD1.

For the sake of probing the surface properties of TiD1 catalyst, *in situ* FTIR with a heating attachment was employed to study the free hydroxyl groups. The spectra shown in Figs. 9a–9c were collected at different temperatures, 25, 200, and 300°C, respectively. Spectrum *d* was obtained after the sample had been heated at 300°C for half an hour. The intensity of stretching vibrations of hydroxyl groups increases with increasing temperatures. An obvious peak at 3633 cm^{-1} is shown when the sample is heated up to 300°C. At the same temperature after half an hour, the hydroxyl group band becomes intense. This indicates that free hydroxyl groups are observed in these IR measurements. Correspondingly, the vibrations of molecular water become weak as temperature is increased. The results suggest that water is driven off of the catalyst at high temperature. Based on this finding, it turns out that the free hydroxyl group band is superimposed on the peak of molecular water because plenty of water is adsorbed on sample TiD1 at room temperature. Indeed, the hydroxyl groups do exist on the titania surface. Yates (31) also showed that molecular water was removed at 350°C by evacuation, but that surface −OH groups were still present.

Moreover, water was readsorbed on sample TiD1 after the temperature dropped to room temperature. This result is not shown. Hence, desorption and adsorption of water in the temperature range 25 to 300°C are reversible processes. The same situations are applicable to sample TiC1.

Figure 10 shows the spectra of TiD1 before and after reaction. The marked peak in the 1423 cm^{-1} region is assigned to carbonate. The two shoulders (1683 and 1362 cm^{-1}) may be due to a small proportion of bicarbonate species

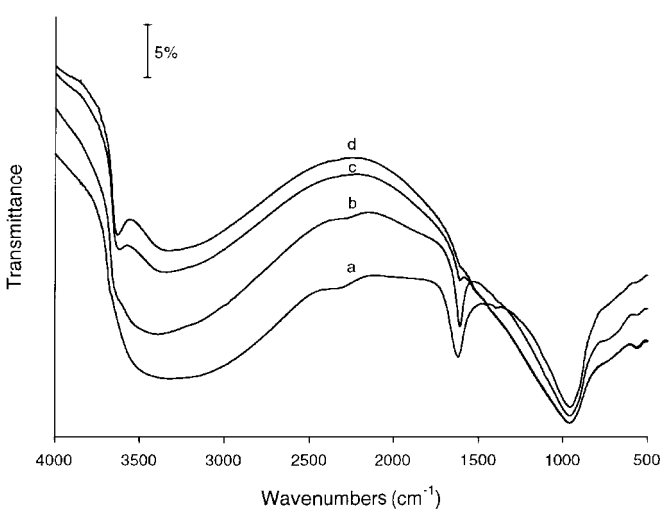

FIG. 9. *In situ* FTIR spectra collected at different temperatures for sample TiD1, (a) RT, (b) 200°C, (c) 300°C, (d) 300°C, after half an hour.

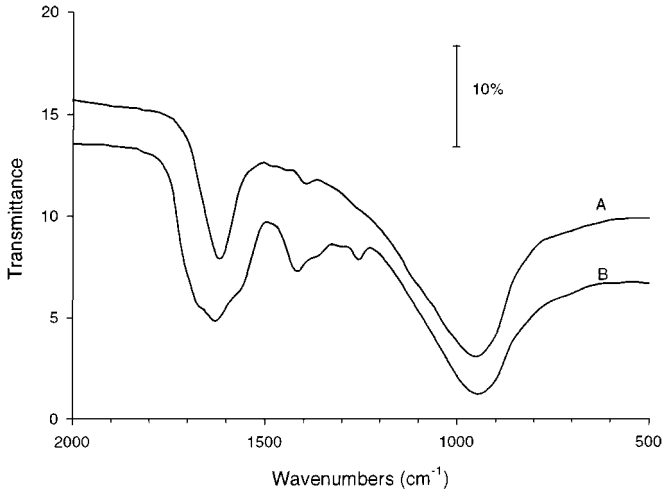

FIG. 10. Diffusion reflectance FTIR spectra of TiD1, (a) before reaction, (b) after reaction in dry conditions.

on the surface (32). According to Yates (31), the shoulder at 1560 cm^{-1} could be due to CO_2^- species. The band at 1260 cm^{-1} is difficult to assign since it does not fall into either the CO_3^{2-} or the HCO_3^- region. Larson *et al.* (15) reported that adsorbed intermediates occur on TiO_2 surfaces in the oxidation of aromatics using temperature-programmed oxidation and desorption (TPO, TPD) techniques.

Figure 10 also implies that 1-butene does not appreciably adsorb on titania since no characteristic groups of 1-butene are visible on the used catalyst. These findings are in agreement with the work of McClintock and Richie (21), who confirmed that olefins were adsorbed irreversibly on TiO_2 catalysts upon illumination, but that adsorption did not occur in the absence of UV light.

DISCUSSION

Role of Water

For photocatalytic reactions proceeding in aqueous solutions, the effects of water concentration on reaction rates are miniscule since the catalyst surface is saturated with water. For gas–solid reactions, however, reactivity of catalysts is strictly related to water vapor. Anpo *et al.* (8) propose that the adsorption of water onto TiO_2 and ZnO causes structural changes in surface band bending, which unfavorably accelerates the recombination of photogenerated electrons and holes, and thus gives rise to low photoefficiency. In an alternative explanation, Phillips and Raupp (9) suggest that water is used to supply hydroxyl groups, which are consumed by trapping holes to generate ·OH radicals in the process of reaction. Yet, water itself can compete with reactants for adsorption on active sites. In general, water plays a double role in gas-phase reactions, as a stabilizer and as an

inhibitor. At lower water concentrations, a delicate balance among, desorption–consumption–adsorption is established to yield a high and steady oxidation rate. At higher water levels, the equilibrium shifts toward water consumption and photoactivity degrades.

This explanation is substantiated in our study. The FTIR results (Figs. 8 and 9) show that the catalysts inherently contain adsorbed water. In the initial stages of the reaction, molecularly adsorbed water is dissociated to form hydroxyl groups. Oxidation rates of 1-butene can be maintained at a high level. With the depletion of adsorbed water, photoactivity of each catalyst falls. At steady state, a balance of consumption and replenishment of water is achieved since the feed stream is not absolutely dry and water can be generated from the oxidation of 1-butene. Figure 2 shows that a water concentration of 2,250 ppm is enough to drive the reaction. However, higher water concentrations inevitably lead to the competitive adsorption of water with 1-butene. This significantly inhibits the oxidation rate of 1-butene.

Some authors have quantitatively reported the effect of humidity on photoactivity. Dibble and Raupp (33) found that the reaction order with respect to water varied with water mole fraction (from zero order to −3 order). Ollis (10) reported that the relationship between the oxidation rates of 1-butanol and water was expressed as

$$r = r_0/(1 + K_H[H_2O]^{\beta}), \quad [3]$$

where $\beta = 1.7$. In our previous work which involved oxidation of 1-butene on SnO_2 and TiO_2, we observed that β was close to 1 by applying the Langmuir–Hinsheldwood model. In the present study, the dependence of rate on the water concentration may be described by the relationship

$$r = r_0 \exp[-kC_w]. \quad [4]$$

Mathematically, this regression is more accurate than Eq. [3] although no mechanism is directly associated with this empirical formula.

Plotting $\ln(r)$ against $-C_w$, we can obtain a straight line for each sample. The k and r_0 can be computed from the slope and intercept of the straight line; r_0 is considered to be the oxidation rate under the condition that the feed stream is absolutely free of water ($C_w = 0$), and k is an influential factor related to water vapor in the flowing stream. As the k value increases there is a stronger effect of humidity on the reactivity of the catalysts. When data of Figs. 1–6 are retreated by applying Eq. [4], the coefficients of r_0 and k for each catalyst can be obtained and are given in Table 3.

Equation [4] reveals that the oxidation rate of 1-butene for these catalysts decreases exponentially as the water concentration increases in the feed stream. Thus, water is a powerful inhibitor for the oxidation of 1-butene. Table 3 shows that the initial oxidation rates (r_0) of each catalyst are higher than the corresponding values for TiA, TiB1, TiC1, and TiD1 (Fig. 1). This could be ascribed to the presence of trace amounts of water vapor, arising from carrier gases and the product of the reaction itself. Water concentrations under such circumstances are beyond the detection limits of the instrument.

TABLE 3

Best-Fit Model Parameters for the Effects of Humidity on Oxidation Rates of 1-Butene (Equation: $r = r_0 \exp[-kC_w]$)

Catalyst	r_0 (μmol/h cm^2)	k ($\times 10^4$ ppm^{-1})	R^2
TiA	0.274	1.57	0.953
TiB1	0.185	2.05	0.977
TiB2	0.170	1.84	0.945
TiC1	0.534	2.75	0.981
TiC2	0.493	1.82	0.994
TiD1	0.799	3.04	0.983
TiD2	0.852	2.63	0.981
TiD3	0.796	1.77	0.971
TiD4	0.759	2.08	0.982

Among each set of catalysts, increases in calcination temperature can reduce k value. In other words, calcination temperature enhances the resistance of catalysts against the effects of humidity. Reduction of the k value on the TiD4 sample (calcined at 400°C) is probably due to a phase transformation indicated in the XRD data. The k values are very similar for all catalysts. For instance, TiB2, TiC2, and TiD3 samples calcined at 300°C are all very similar.

Effects of Particle Size

The significant differences in properties of these catalysts are due to the large specific surface areas and smaller average particle sizes of synthesized TiO_2 as compared to P-25 TiO_2. Catalysts with a diameter of 5–6 nm exhibit high oxidation rates of 1-butene, while low oxidation rates are obtained on TiA and TiB2, whose particle sizes are 28 nm and less than 3 nm, respectively.

Some authors have reported a dependence of photoefficiency on the particle size of semiconductors. By studying ultrasmall particles in colloids, Hoffman *et al.* (34, 35) suggest that particles with diameters between 1 and 10 nm are referred to as quantum-sized particles (Q-sized particles, or nanoscale particles). Mills *et al.* (3) propose that Q-sized particles are typically 5–20 nm in diameter. These ultrasmall particles fall into the transition region between molecular and bulk semiconductor properties. Thus, they exhibit unique photochemical properties. By studying photocatalytic hydrogenation of CH_3CCH with H_2O on small particle TiO_2 catalysts, Anpo *et al.* (26) suggest that the enhancement in photoactivity is closely associated with quantum size effects, which is verified by the observation of considerable blue shifts.

The most competitive process with the oxidation of organic pollutants is the recombination of electrons and holes

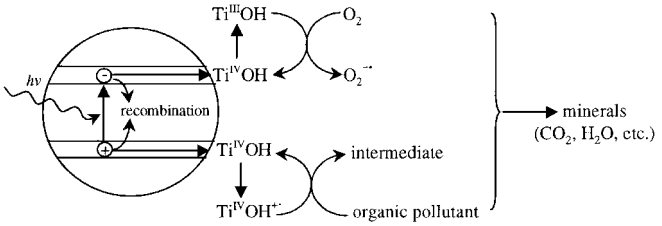

FIG. 11. The primary processes suggested by Hoffmann (2) and Mills (3) for the photodecomposition of organic pollutants. The steps from intermediates to final products are still under debate (39).

generated in semiconductors after the absorption of photons (Fig. 11). Usually, electrons and holes need to diffuse to catalyst surfaces, where they are captured by electron and hole acceptors. If the dimensions of nanoscale particles are so small that the diffusion of electrons and holes to the surfaces is faster than the recombination process, the photoefficiency would be enhanced by employing such ultrasmall particles. In comparison with bulk semiconductors, the nanoscale semiconductor retards the electron–hole recombination via charge carrier trapping. Miller *et al.* (3) predict that it would be possible to obtain quantum yields approaching unity with nanoscale particles. Our work shows that nanoscale particles (TiC and TiD series catalysts) are more photoefficient than P-25 TiO_2 with an average diameter of 28 nm. This is consistent with ideas of Miller *et al.* (3). According to this trend, higher photoactivity is expected to be obtained on TiB2 or TiB1. However, the experimental results are in contradiction with this speculation. The crystalline structure is likely another factor influencing photoactivity since these two samples mainly consist of amorphous TiO_2, which is not a good photocatalyst.

The main contribution of nanoscale particles to surface reactions is ascribed to the enhancement of active sites due to large surface areas. In our present study, a surface area of 100 to 160 m^2/g is the optimal value for the decomposition of 1-butene. Catalysts with too high or too low surface areas are not good candidates for decomposition of air contaminants.

In addition, blue shifts caused by nanoscale effects enhance the band gap, which in turn increases the redox potential (36). Therefore, nanoscale particles should be more photoactive than macrocrystalline semiconductor particles. In comparison to the TiO_2 materials synthesized here, the crystallinity of anatase is also important to obtain high photoefficiency, in addition to the requirement of appropriate particle size. This is in agreement with reports of Mills *et al.* (37) and Martin *et al.* (38), who claim that anatase is much more photoactive than rutile.

Deactivation

As described in the results section, the used TiO_2 catalysts turned pale yellow after each test. No partially oxidized products were directly detected despite the FTIR evidence that carbonate or bicarbonate species were chemisorbed on catalyst surfaces. The deactivation shown in Fig. 1 is mainly due to dry conditions. Therefore, the accumulation of carbonate species on active sites results in the deactivation of TiO_2 photocatalysts in this case. This explanation is in agreement with the reports of Cunningham *et al.* (14) and Larson *et al.* (15), who suggest that the presence of organic compounds is responsible for deactivation in gas–solid reactions. However, for the oxidation of 1-butene, no obvious deactivation was observed as long as the flowing stream contained the appropriate amount of water. Severe deactivation was seen for the oxidation of toluene in our study even though the same TiO_2 series catalysts were applied. Therefore, the deactivation of these catalysts is dependent on the nature of the reaction.

CONCLUSIONS

Our study shows that catalyst properties, such as photoactivity, size of crystallites, surface areas, and surface conditions, are all affected by preparation methods. The sol–gel technique with assistance of acids (especially HCl) can be utilized to enhance the oxidation rate of 1-butene. In the reaction of oxidizing 1-butene, water plays two different roles, as a stabilizer by replenishing hydroxyl groups at low humidity, and as a strong inhibitor by competing with 1-butene for adsorption of active sites. In the range 2,250 to 12,000 ppm, water exponentially decreases the photoactivity of the TiO_2 series catalysts. A calcination temperature of 300°C can help improve the resistance of TiO_2 catalysts against the effects of humidity. However, higher calcination temperature unfavorably results in phase transformation from anatase to rutile. Amorphous and rutile-typed TiO_2 are less photocatalytically active.

BET measurements and XRD patterns combined with the Scherrer equation show that the catalysts have surface areas of $100 \sim 160$ m^2/g and average diameters of $5 \sim 6$ nanometers, contain anatase, and show high activity. Quantum size effects, which lead to high surface areas and blue shifts and diminish electron–hole recombination, are used to explain these experimental results. *In situ* FTIR data show the presence of hydroxyl groups and large amounts of adsorbed water on TiO_2. The deactivation of TiO_2 photocatalyst under dry conditions results from the accumulation of carbonate species on active sites. No apparent deactivation occurred in the presence of trace amounts of water vapor in the feed stream.

ACKNOWLEDGMENTS

We acknowledge United Technologies Research Center for use of the BNK instrument. We also thank Dr. Leon L. Shaw and Mr. Zhengguo Yang in the Institute of Materials Science at the University of Connecticut for BET measurements.

REFERENCES

1. Fox, M. A., and Dulay, M. T., *Chem. Rev.* **93**, 341–357 (1993).
2. Hoffmann, M. R., Martin, S. T., Choi, W., and Bahnemann, D. W., *Chem. Rev.* **95**, 69–96 (1995).
3. Mills, A., and Le Hunte, S., *J. Photochem. Photobiol. A Chem.* **108**, 1–35 (1997).
4. Ollis, D. F., and Al-Ekabi, H., Eds., "Photocatalytic Purification and Treatment of Water and Air." Elsevier, Amsterdam, 1993.
5. Ohko, Y., Hashimoto, K., and Fujishima, A., *J. Phys. Chem. A* **101**, 8057–8062 (1997).
6. Martin, S. T., Herrmann, H., Choi, W., and Hoffmann, M. R., *Trans. Faraday Soc.* **90**, 3315–3323 (1994).
7. Martin, S. T., Herrmann, H., and Hoffmann, M. R., *Trans. Faraday Soc.* **90**, 3323–3330 (1994).
8. Anpo, M., Chiba, K., Tomonari, M., Coluccia, S., Che, M., and Fox, M. A., *Bull. Chem. Soc. Jpn.* **64**, 543–551 (1994).
9. Phillips, L. A., and Raupp, G. B., *J. Mol. Catal.* **77**, 297–311 (1992).
10. Peral, J., and Ollis, D. F., *J. Catal.* **136**, 554–565 (1992).
11. Obee, T. N., and Brown, R. T., *Environ. Sci. Technol.* **29**, 1223–1231 (1995).
12. Pruden, A., and Ollis, D. F., *J. Catal.* **82**, 404–417 (1983).
13. d'Hennezel, O., and Ollis, D. F., *J. Catal.* **167**, 118–126 (1997).
14. Cunningham, J., and Hodnett, B. K., *J. Chem. Soc. Faraday Trans. I* **77**, 2777–2801 (1981).
15. Larson, S. A., and Falconer, J. L., *Catal. Lett.* **44**, 57–65 (1997).
16. Jacoby, W. A., Blake, D. M., Noble, R. D., and Koval, C. A., *J. Catal.* **157**, 87–96 (1995).
17. Obee, T. N., and Hay, S. O., *Environ. Sci. Technol.* **31**, 2034–2038 (1997).
18. Cullity, B. D., "Elements of X-Ray Diffraction." Addison-Wesley, Reading, MA, 1978.
19. Che, M., and Bennett, C. O., *Adv. Catal.* **36**, 55–172 (1989).
20. Matthews, R. W., and McEvoy, S. R., *J. Photochem. Photobiol. A Chem.* **66**, 355–366 (1992).
21. McClintock, I., and Ritchie, M., *Trans. Faraday Soc.* **61**, 1007–1016 (1965).
22. Anpo, M., *Res. Chem. Intermed.* **11**, 67–106 (1989).
23. Abrahams, J., Davidson, R. S., and Morrison, C. L., *J. Photochem.* **29**, 353–361 (1985).
24. Fu, X., Clark, L. A., Yang, Q., and Anderson, M. A., *Environ. Sci. Technol.* **30**, 647–653 (1996).
25. Canela, M. C., Alberici, R. M., and Jardim, W. F., *J. Photochem. Photobiol. A Chem.* **112**, 73–80 (1998).
26. Anpo, M., Shima, T., Kodama, S., and Kubokawa, Y., *J. Phys. Chem.* **91**, 4305–4010 (1987).
27. Anderson, C., and Bard, A. J., *J. Phys. Chem.* **99**, 9882–9885 (1995).
28. Primet, M., Pichat, P., and Mathieu, M.-V., *J. Phys. Chem.* **75**, 1216–1220 (1971).
29. Walrafen, G. E., *J. Chem. Phys.* **40**, 3249–3256 (1964).
30. Walrafen, G. E., *J. Chem. Phys.* **36**, 1035–1043 (1962).
31. Yates, D. J. C., *J. Phys. Chem.* **65**, 746–753 (1961).
32. Miller, F. A., and Wilkins, C. H., *Anal. Chem.* **24**, 1253–1294 (1953).
33. Dibble, L. A., and Raupp, G. B., *Catal. Lett.* **4**, 345–354 (1990).
34. Hoffman, A. J., Yee, H., Mills, G., and Hoffmann, M. R., *J. Phys. Chem.* **96**, 5540–5546 (1992).
35. Hoffman, A. J., Mills, G., Yee, H., and Hoffmann, M. R., *J. Phys. Chem.* **96**, 5546–5552 (1992).
36. Dagan, G., Sampath, S., and Lev, O., *Chem. Mater.* **7**, 446–453 (1995).
37. Mills, A., Morris, S., and Davies, R., *J. Photochem. Photobiol. A Chem.* **70**, 183–191 (1993).
38. Martin, S. T., Morrison, C. L., and Hoffmann, M. R., *J. Phys. Chem.* **98**, 13695–13704 (1993).
39. Heller, A., *Acc. Chem. Res.* **28**, 503–508 (1995).